First-principles calculations of the electronic structure and pressure-induced magnetic transition in siderite $FeCO_3$

H. Shi,[1] W. Luo,[1,2,*] B. Johansson,[1,2] and R. Ahuja[1,2]

[1]*Department of Physics, Condensed Matter Theory Group, Uppsala University, P.O. Box 530, SE-751 21 Uppsala, Sweden*

[2]*Applied Materials Physics, Department of Materials and Engineering, Royal Institute of Technology (KTH), SE-100 44 Stockholm, Sweden*

(Received 15 May 2008; published 17 October 2008)

Rhombohedral siderite $FeCO_3$ has been studied by using density-functional theory with the generalized gradient approximation (GGA). In order to take into account the strong on-site Coulomb interaction U present in $FeCO_3$, we also performed the GGA+U calculations. We observe a pressure-induced magnetic transition (high spin→low spin) at pressures of 15 and 28 GPa, which are underestimated with respect to the experiment, for the GGA and GGA+U calculations, respectively. This phase transition was with a volume collapse of 10% around, also accompanied by increases in bulk modulus, Young's modulus and sound velocity. The electronic density of states and charge-density calculations revealed that the magnetic transition was due to the pressure-induced Fe 3d electron delocalization.

DOI: 10.1103/PhysRevB.78.155119 PACS number(s): 31.15.A−, 75.30.Kz, 91.60.Gf

I. INTRODUCTION

Earth's mantle is a thick rocky shell comprising approximately 70% of earth's volume. It is predominantly solid and overlies the earth's iron-rich core. So the properties of iron in various minerals under high pressure, matching to the condition at the inner earth, arouse special interest. On the other hand, it is well known that several basic properties of materials, such as crystalline and electronic structures, and the dielectric, magnetic, thermodynamical, and transport properties are modified when high pressure is applied. Transition-metal ions with unfilled d shells are especially prone to electronic phase transitions at high pressures. Especially the iron magnetic states in ferropericlase[1–4] and silicate perovskites[5] under high pressure have been extensively studied, since they directly influence the earth's lower mantle properties. Recently, the high-pressure x-ray emission spectra (XES) work by Lin *et al.*[6] showed the sound velocity increase in mid-lower mantle due to the $(Mg_{0.93}Fe_{0.07})O$ HS-to-LS (high-spin to low-spin) transition. The latest study regarding $(Mg_{0.83}Fe_{0.17})O$ by Crowhurst *et al.*[7] also revealed a negative anomaly for sound velocities in the HS-to-LS coexist layer of lower mantle. Ding *et al.*[8] recently reported a pressure-induced HS to intermediate-spin (IS) transition at 12–16 GPa for magnetite (Fe_3O_4) by using synchrotron-based x-ray magnetic circular dichroism (XMCD) measurements. These mineral physics studies have prompted geophysicists and geodynamicists to re-evaluate the state of the lower mantle in terms of spin-pairing phenomena. Experimentally, pressure-induced magnetic transitions have been observed in various transition-metal bearing compounds[1,2,4,9–16] using high-resolution XES. Theoretically, the magnetic transitions also have been approached by using crystal-field theory,[17] charge-transfer multiplet calculations,[18–20] as well as density-functional theory (DFT) calculations. Cohen *et al.*[21] investigated high-pressure magnetism in transition-metal oxides within the generalized gradient approximation (GGA) method by considering the important d electrons as bandlike under pressure. Recently, an improved method, namely, LDA+U (Ref. 22–24) or including the GGA approach,[25–27] treating the d-electron correlation effects at pressures, has been adopted widely.

For many iron minerals exhibiting a pressure-induced HS-to-LS transition, the understanding of magnetic transition is significant. As an extension of these magnetic-transition studies on iron compounds, we have now extended these investigations to siderite $FeCO_3$ mineral. Siderite is a yellowish brown mineral composed of iron carbonate $FeCO_3$. It commonly occurs in sedimentary iron ores and is a valuable iron mineral since it is 48% iron and contains no sulfur or phosphorus. Its crystal structure belongs to the hexagonal system and is rhombohedral in shape. As a member of the calcite family, siderite has $R\bar{3}c$ space group with two molecular formula units per unit cell, as one can see in Fig. 1. The Fe^{2+} ions are octahedrally coordinated by six oxygen atoms. The details of its crystalline structure have been reported by Wyckoff,[28] Cowley,[29] and Rao *et al.*[30] However, according to our knowledge, relatively few experiments and theoretical works regarding the high-pressure properties of $FeCO_3$ exist. Santillán and Williams[31] found that the $FeCO_3$ calcite crystal structure is stable up to 50 GPa at room temperature by using infrared spectroscopy and high-pressure x-ray diffraction methods. The magnetic state of iron in siderite $FeCO_3$ under high pressure using $K\beta$ x-ray emission spectroscopy has been studied by Mattila[32] recently. Mattila's work revealed that the Fe^{2+} ion is in the HS (S=2)

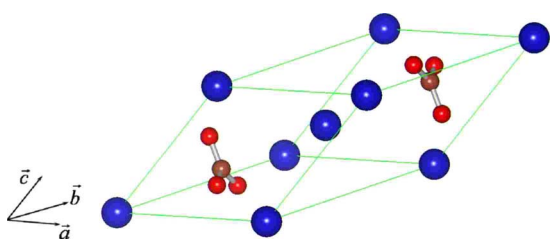

FIG. 1. (Color online) Primitive unit cell of $FeCO_3$. Blue, brown, and red spheres represent Fe, C, and O atoms, respectively.

ground state at low pressure and loses its magnetic moment and undergoes a transition into a nonmagnetic LS ($S=0$) phase at around 50 GPa. However, Mattila's work didn't mention the information about other properties at transition pressure, such as a volume collapse, bulk modulus, speed of sound, and changes in optical properties.

Ab initio simulation technique is a reliable tool for investigating the electronic structure and magnetic properties of materials under extreme conditions, such as high pressure and temperature.[33] By using first-principles calculations, one can go far beyond the pressure and temperature ranges achieved experimentally. One important area, the crystalline structures and phase transformations at high pressure of earth's interior constituents, can be dealt with using first-principles calculations. In this paper, the pressure-induced magnetic phase transition, electronic structure of $FeCO_3$, as well as geometrical structure have been studied using first-principles method.

II. CALCULATION METHODS

We have studied the high-pressure-induced magnetic transition in $FeCO_3$ by performing first-principles calculations based on the DFT. *Ab initio* simulations were performed using the projector-augmented wave (PAW) method[34] as implemented in Vienna *ab initio* simulation package (VASP) code,[35,36] and the GGA (Ref. 37) was used to describe the electronic exchange-correlation effects. We have chosen the exchange-correlation functional proposed by Perdew *et al.*[37,38] in 1991 using the GGA denoted hereby PW91. For Fe atoms, we have used PAW potentials with the following orbitals treated as valence states: $3s^2 3p^6 3d^7 4s^1$ configuration ($r_{\text{core}}=1.900$ a.u.), where r_{core} is the core radius. The *hard* PAW potentials for C and O were used for calculations in this work. Four and six valence electrons for each C atom ($2s^2 2p^2$, $r_{\text{core}}=1.100$ a.u.) and O atom ($2s^2 2p^4$, $r_{\text{core}}=1.100$ a.u.) were taken into account, respectively. The remaining *core* electrons together with the nuclei were described by pseudopotentials in the framework of the PAW method. The calculations were performed using a cutoff energy of 875 eV and sampling the Brillouin zone with fixed k ($10\times10\times10$) points with the number of 116 irreducible k points.

However, it should be noted that in DFT calculations, the electronic structure of a system with strong electron correlation, such as transition-metal (TM) compounds, is not well described. The local-density approximation (LDA) or GGA often fails to describe systems with strongly correlated d and f electrons. In some cases this can be remedied by introducing a strong intra-atomic (on-site) Coulomb interaction in a Hartree-Fock-like manner as a replacement of the LDA (or GGA) on-site energy. This approach is commonly known as the LDA+U or GGA+U method.[39] There is a simple formulation of the DFT+U method by Liechtenstein[40] and Dudarev *et al.*,[41] where a single parameter U_{eff} determines an orbital-dependent correction to the DFT energy. U_{eff} is generally expressed as the difference between two parameters: the Hubbard U, which is the Coulomb-energetic cost to place two electrons at the same site, and a parameter J representing the screened exchange energy. While U depends on the spatial extension of the wave functions and on screening, J is an approximation of the Stoner exchange parameter and almost constant $J\sim1$ eV.[42] The $U_{\text{eff}}=0$ case represents the DFT limit, and a larger U_{eff} forces a stricter observance of the on-site idempotency, achieved by lowering the one-electron potential locally for the specified orbitals of the metal atoms (e.g., Fe d orbitals) and in turn reducing the hybridization with, e.g., O atoms. The parameter $U_{\text{eff}}=4$ eV was used by Ricardo *et al.*[43] for $FeSbO_4$ and Fang *et al.*[22] for FeO calculations. Rollmann *et al.*[27] investigated the structure and magnetic phases of hematite using the GGA+U method with different U (ranging from 1 to 9 eV) and demonstrated that the value of 4 eV is the best one for overall agreement with experiment. In this work, to obtain a more accurate theoretical understanding of the electronic and magnetic properties of $FeCO_3$, we performed the GGA+U calculations with $U=4$, 5, and 6 eV and $J=1$ eV to simulate $FeCO_3$ under pressures and compared with the GGA.

III. RESULTS AND DISCUSSION

A. Crystal structure and pressure-induced magnetic transition

We first performed an optimization of the geometry of the lattice and internal structural parameters within the GGA and GGA+U schemes. Siderite is calcitelike arrangements of Fe^{2+} and CO_3^{2-} ions distorted by spatial requirements of its complex anions, forming a threefold symmetry axes. The symmetry is rhombohedral, with a bimolecular unit, as we can see Fig. 1. Atoms were early found to be in the following positions of D_{3d}^6 ($R\bar{3}c$): Fe: (0, 0, 0); $(\frac{1}{2},\frac{1}{2},\frac{1}{2})$, C: $\pm(\frac{1}{4},\frac{1}{4},\frac{1}{4})$, and O: $\pm(u+\frac{1}{4},-u+\frac{1}{4},\frac{1}{4})$; $\pm(-u+\frac{1}{4},\frac{1}{4},u+\frac{1}{4})$; $\pm(\frac{1}{4},u+\frac{1}{4},-u+\frac{1}{4})$ with an internal structural parameter u that has been determined as 0.27 experimentally by Wyckoff.[28] By fitting the calculated energies versus unit-cell volumes, we can determine the equation-of-state parameters (the zero pressure lattice parameters a_0, c_0, where a_0 is the length of the basic vector and c_0 represents the length of the rhombohedral diagonal, see Fig. 1). In the GGA+U (5 eV) calculations, for the HS phase, which is stable under low pressures, our optimized volume of unit cell is 99.46 Å^3, overestimating the experimental value of 97.63 Å^3 by around 1.9%, as we can see in Table I and Fig. 2. Our theoretical optimized lattice constants a_0 and c_0 equal to 5.786 and 15.278 Å, being in good agreement with the experimental values of 5.795 and 15.370 Å,[28] respectively. A more visual parameter describing the shape of the unit cell, the angle α between basic vectors, is 48.46°, overestimating the experiment (47.75°) by 1.5%. The internal parameter u, determining the positions of the threefold O atoms, is 0.272, being in good agreement with the experimental result of 0.27.[28] For the GGA calculations, a_0 and c_0 are both underestimated by 0.4% and 0.8%, respectively. However, the optimized unit volume and the angle α are more close to the experimental values. We should note here that although the experimental a_0 and c_0 are both larger than those of our theoretical results, the experimental volume is smaller, and the reason is due to the angle α or the c/a ratio indicating the shape of the primitive cell.

TABLE I. Theoretical and experimental (Ref. 28) unit-cell parameters and atomic positions of $FeCO_3$. a_0 is the optimized length of the basic vector; c_0 represents the optimized length of the rhombohedral diagonal, V_0 indicates the volume of the equilibrium state, and α is the angle between basic vectors.

	a_0 (Å)	c_0 (Å)	V_0 (Å^3)	α	u
GGA	5.770	15.252	98.40	48.35°	0.274
GGA+U (4 eV)	5.782	15.269	99.39	48.49°	0.272
GGA+U (5 eV)	5.786	15.278	99.46	48.46°	0.272
GGA+U (6 eV)	5.781	15.261	99.24	48.47°	0.272
Experiment	5.795	15.370	97.63	47.75°	0.27

As a whole, here we can conclude that our theoretical calculations within the GGA and GGA+U methods for the geometry of $FeCO_3$ are both in good agreement with experiment.

Figure 3 shows the calculated distortions for the HS and LS phases of $FeCO_3$ as a function of pressure. It is shown clearly that the rhombohedral unit cell is compressed in the $c(z)$ direction with increasing pressure. The c/a ratio changes from 2.64 (at 0.6 GPa) to 2.58 (at 32 GPa). According to our calculations, the lattice constants a and c at the pressure of around 32 GPa, closing to the phase-transition point (28 GPa), are 5.19 and 13.37 Å, reduced by 10.4% (0.60 Å) and 12.5% (1.91 Å), respectively. However, the distance between C and O atoms in one CO_3^{2-}-ion group changes from 1.293 to 1.275 Å, decreasing only by 1.4%. This suggests that the internal structural parameter (and hence the C-O distance) shows a less dependence on increasing pressure.

For the GGA+U (5 eV) case, when we consider lower volumes, we observe a collapse of the magnetic moments, from the HS to LS state, which occurs at around 79.3 Å^3. By placing a common tangent to the HS and LS curves, we obtain a value for the pressure, for which an HS→LS transition will occur, of around 28 GPa. The corresponding volume collapse is 9.7%. This volume collapse can be explained by the fact that the delocalized Fe 3d electrons form electron pairs leading an increase in attraction between neighbor Fe atoms. The experimental HS→LS transition point was determined at 50 GPa by Mattila[32] using XES. When comparing our result to the experiment, we note that we underestimate this phase-transition pressure considerably, unlike previous geometry calculations. On the other hand, the GGA method gives the magnetic-transition pressure of around 15 GPa, accompanying a more volume collapse of 12.5%, and underestimates the experimental value by 70%. It is shown clearly that the GGA+U method induces a transition-pressure shift to higher pressures and gives a better result. Rollmann *et al.*[27] also demonstrated that when the GGA+U formalism is

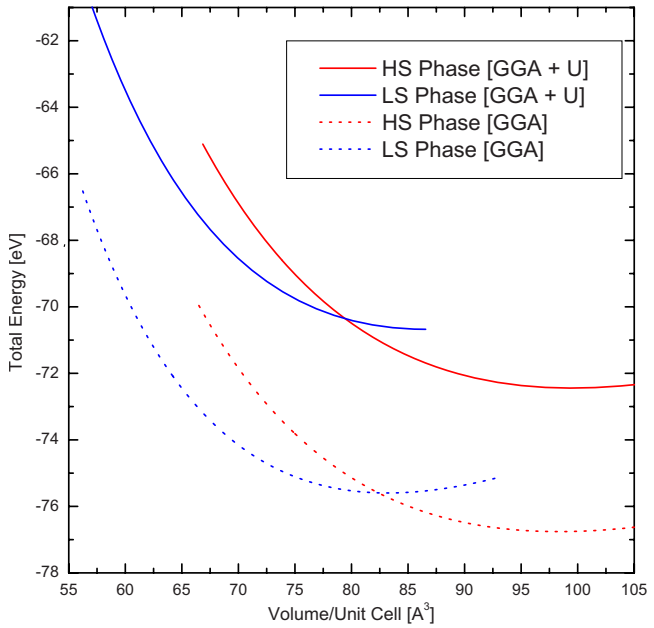

FIG. 2. (Color online) Total energies as a function of the unit volume for the GGA and GGA+U (5 eV) calculations. The least-squares-fitted curves to Birch-Murnaghan equation of state are shown.

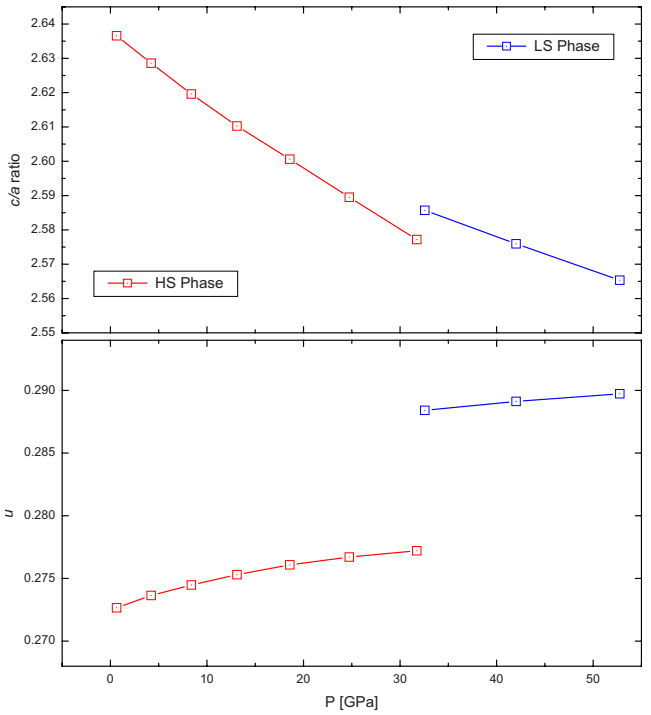

FIG. 3. (Color online) Variation of the c/a ratio and internal parameter u with pressures in the HS and LS phases within the GGA+U (5 eV) calculations.

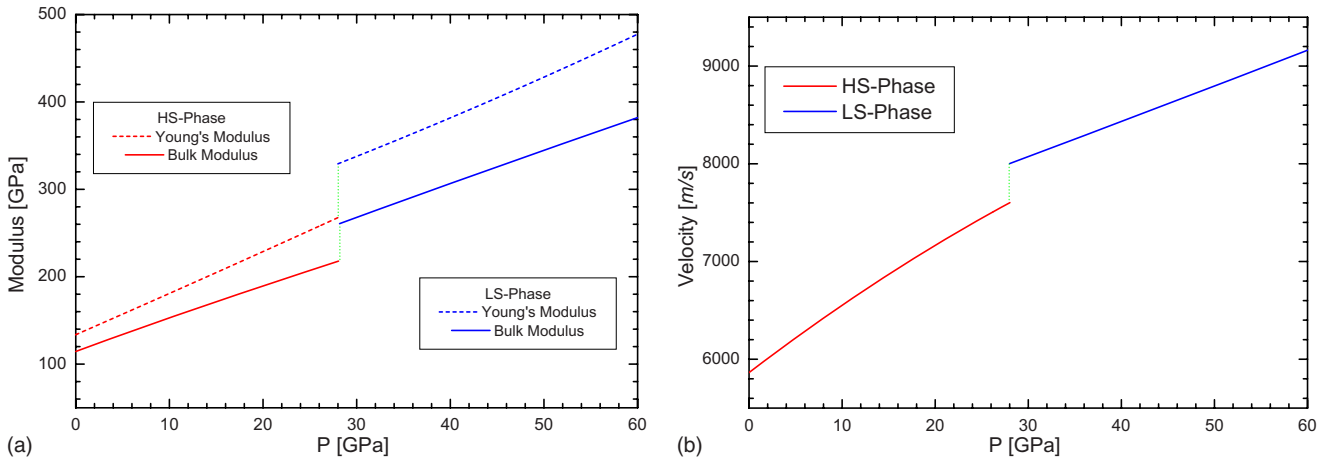

FIG. 4. (Color online) Variation with pressure of bulk modulus B, Young's modulus Y, and sound velocity v of the HS and LS phases within the GGA+U (5 eV).

applied, the observed transition is shifted to higher pressures with increasing U and eventually disappears for large values of U. We also calculated the phase-transition pressure with $U=6$ eV and found that the transition-pressure (30 GPa) shift is only about 2 GPa to higher pressures, still being far from the experimental value, and the calculations for the geometry of $FeCO_3$ are close to previous calculations with $U=5$ eV. It is suggested that the value of U should be very large if we want to get a better phase-transition pressure within this GGA+U method for $FeCO_3$ calculations, but maybe very high value of U will be not physical. Table I also lists the geometric parameters for the $U=4$ eV case. From Table I, we can conclude that both the GGA and GGA+U methods do not show any significant changes for structural calculations. The corresponding phase-transition pressure in the $U=4$ eV case is around 25 GPa. Finally, the geometry calculations for the LS states near the transition point show that there is a distortion mutation at the transition point (Fig. 3). For the GGA+U (5 eV) calculations, angle α is reduced from 52.5° to 52° during the HS→LS transition. However, the internal structural parameter of the C-O distance is nearly not changed.

B. Bulk modulus, Young's modulus, and speed of sound

By fitting the variation of total energy with volume to Birch-Murnaghan equation of state, we obtained the bulk modulus ($B_0=114$ GPa) and the pressure derivative of the bulk modulus ($B_0'=3.99$), which are in good agreement with the experimental values of 117 and 4 GPa,[31] respectively, within the GGA+U (5 eV). Additionally, we evaluated Young's modulus Y, determining the speed of sound in solids, by calculating the energetic gains of the stretched lattice as a function of the square of the stretching length along the $c(z)$ direction. Figure 4 shows bulk modulus B and Young's modulus Y as functions of pressure. Bulk modulus at the spin-transition pressure changes abruptly from 218 to 261 GPa, with a bulk modulus increase of 43 GPa. Our calculated Y is around 134 GPa for the HS phase under ambient pressure, and at the transition point (around 28 GPa), Y changes from 267 GPa for the HS phase to 329 GPa for the LS phase, with an increase of about 23%. Unfortunately, we did not find the experimental data for Young's modulus of $FeCO_3$ in literature. However, Schmitt *et al.*[44] predicted that $FeCO_3$ should have a similar Young's modulus as FeO (130 GPa), suggesting the rationality of our calculation. We also studied the variation of the speed of sound with pressure for the HS and LS phases, as we can see in Fig. 4. The calculated velocity at ambient condition for the HS phase is around 5860 m/s and the velocity increases with increasing pressure. According to our calculations, there is a change in sound speed between the HS (≈7600 m/s) and LS (≈8000 m/s) phases at the phase-transition pressure, and the gain of velocity is about 400 m/s, increasing by 5%. The increase in sound speed between the HS and LS phases is also in accordance with the work of Lin *et al.*,[6] which indicated faster sound velocities for the LS phase relative to the HS ferropericlase.

C. Electronic structure

In order to analyze electronic properties of $FeCO_3$, we have calculated the density of states (DOS) for the HS and LS phases. The spin-polarized total and partial DOSs, calculated in the GGA+U scheme with $U=5$ eV, are shown in Figs. 5 and 6. For the HS phase at lower pressure of 0.6 GPa, the band gap is 1.3 eV. The corresponding value for the HS phase at 32 GPa is 0.9 eV. From Fig. 5, we can conclude that for the spin-up case, the Fe $3d$ and O $2p$ orbitals form the top of valence bands, indicating a strong Fe-O $3d-2p$ hybridization characteristic near Fermi energy, and O $2p$ and C $2p$ orbitals do the most contributions to the bottom of conduction bands, whereas for the spin-down case, the top of valence bands mainly consists of O $2p$ orbitals and the Fe $3d$ orbitals form the bottom of the conduction bands. When comparing the spin-up DOS of the lower-pressure (0.6 GPa) case to that of the higher-pressure (32 GPa) case near Fermi level, we can see that the Fe $3d$-orbital contribution to the top of valence bands in the high-pressure case is more pronounced than in the lower-pressure case. This can be ex-

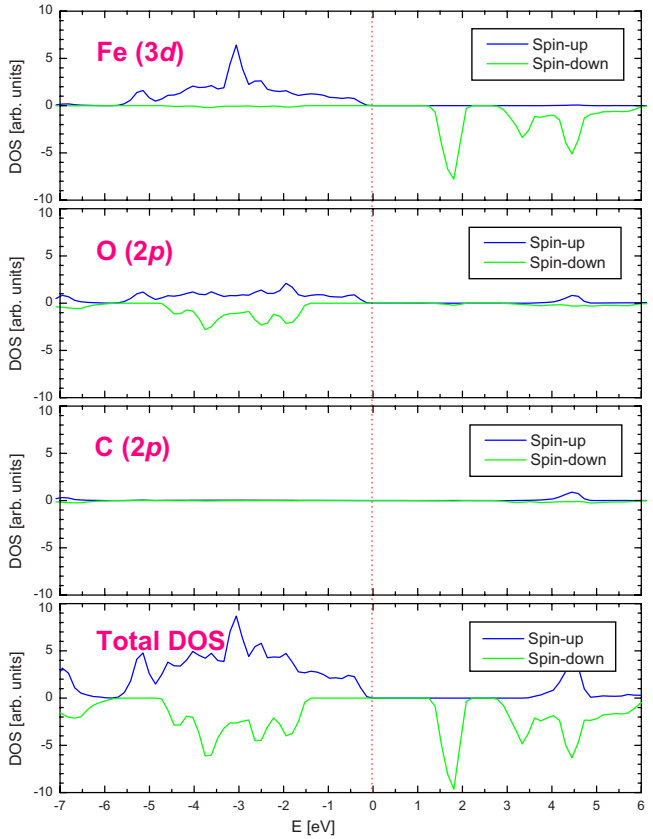

FIG. 5. (Color online) Total and partial DOSs for the HS phase of $FeCO_3$ at 0.6 GPa (low pressure), calculated within the GGA $+U$ (5 eV). The positive and negative curves indicate the spin-up and spin-down states, respectively.

plained by the fact of more delocalized d electrons under higher pressure.

The calculated DOS for the LS phase at 32 GPa is also shown in Fig. 6. We can see clearly, unlike the HS phase, that the top of valence bands and the bottom of conduction bands both mainly consist of Fe 3d orbitals. The band gap is 1.9 eV. For the Fe 3d DOS of the HS phase, there is a small peak located at about −3 eV below the Fermi level, and the DOS curve is broad. However, for the LS phase, the Fe 3d DOS curve is sharper and has an obvious shift to the Fermi level, indicating a delocalization of Fe 3d electrons.

Figure 7 shows the total and partial DOSs for the HS phase of $FeCO_3$ at lower pressure of 0 GPa within the GGA calculations. Band gap of 0.4 eV is clearly visible. For comparison, this value is smaller than the corresponding value in the GGA+U (5 eV) case (1.3 eV in the HS phase at low pressure of 0.6 GPa). The disagreement with the GGA+U method may be traced back to the fact of lowering the one-electron potential locally for the Fe 3d orbitals and in turn reducing the hybridization with O 2p orbitals in the GGA $+U$ scheme. Unlike the GGA+U calculations, the top of the valence bands mainly consists of Fe 3d orbitals. Whereas in the GGA+U case, we can observe Fe 3d states and O 2p states in comparable amounts at the upper edge of the valance bands.

The delocalization of Fe 3d electrons with increasing pressure, leading to the HS→LS transition, can also be seen

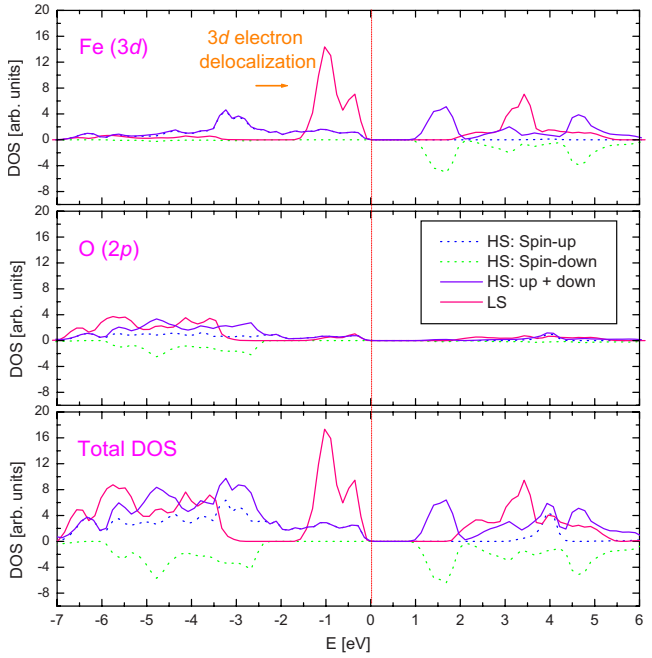

FIG. 6. (Color online) Total and partial DOSs for the HS and LS phases of $FeCO_3$ at 32 GPa (high pressure), calculated within the GGA+U (5 eV). The positive and negative curves indicate the spin-up and spin-down states, respectively. The dot line represents the sum of spin up and spin down.

by analyzing the electronic charge density. In Fig. 8, the projections of the charge density in the (100) plane crossing at the Fe atom site for both the HS and LS phases are shown. Here we should note that the Fe atoms in the charge-density

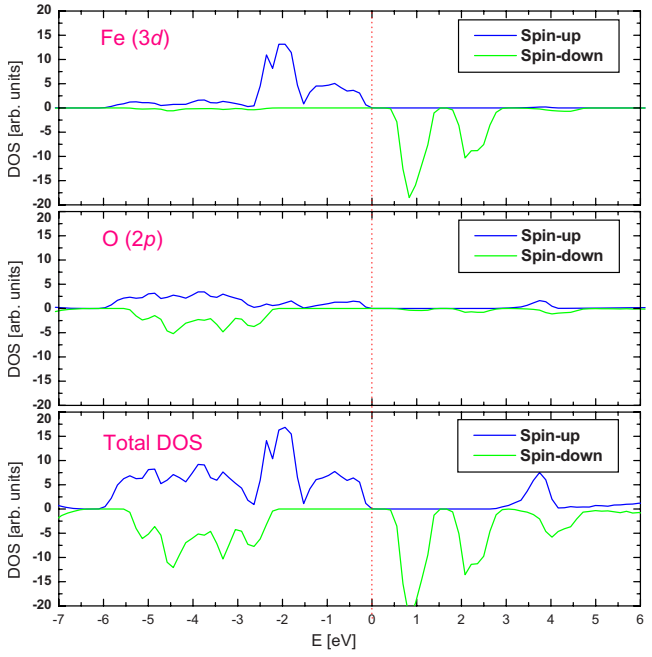

FIG. 7. (Color online) Total and partial DOSs for the HS phase of $FeCO_3$ at 0 GPa (low pressure), calculated within the GGA. The positive and negative curves indicate the spin-up and spin-down states, respectively.

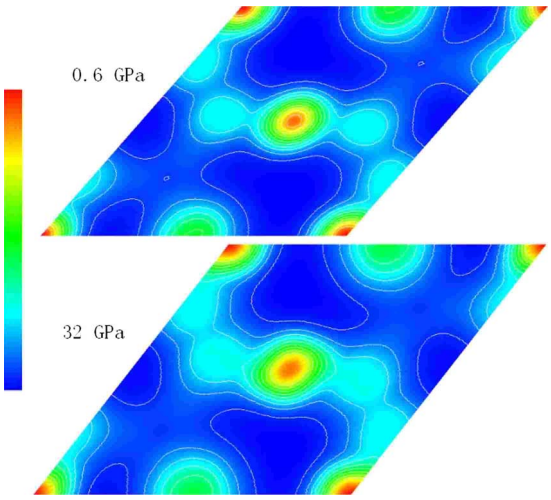

FIG. 8. (Color online) Projections of the charge density in the (100) plane crossing at Fe atom site for the HS and LS phases in the GGA+U (5 eV) case. Upper map: HS phase at 0.6 GPa (low pressure); lower map: LS phase at 32 GPa (high pressure). The red regions denote Fe atoms.

map (Fig. 8) are not in one plane crossing the center Fe atom, being due to the projections. For the HS phase at 0.6 GPa (low pressure), there are few 3d electron overlaps between two neighbor Fe atoms. For the LS phase at 32 GPa (high pressure), the projections of the charge density reveal obvious 3d bonding between neighbor Fe atoms. According to the Pauli exclusion principle, the high-spin state is vanished by paired 3d electrons with decreasing Fe-Fe distance. On the other hand, as mentioned before, there is a mutation of angle α occurring at the phase-transition point. In the HS phase, there are net unpaired electrons localized around Fe atoms, presenting magnetic order, which leads a repulsion between neighbor Fe atoms with respect to the paired-electron case. Therefore, these abrupt changes for the shape of the unit cell and the volume collapse also can be explained by the formation of a new, though not strong, d bond between two neighbor Fe atoms.

IV. CONCLUSIONS

We have calculated structural and electronic properties of rhombohedral siderite $FeCO_3$ for different volumes of the primitive unit cell in the framework of DFT using the GGA and GGA+U. It could be shown that although ground-state geometric properties such as the equilibrium volume, lattice constants a_0 and c_0, and internal structural parameter u agree well with experimental data in both the GGA and GGA+U methods, the HS→LS magnetic-transition pressure is underestimated considerably. Our calculations show that the transition accompanying a volume collapse (12.5% for GGA and 9.7% for GGA+U=5 eV), a cell-distortion mutation, increases in bulk modulus, Young's modulus, and sound velocity, as well as a red shift in the optical gap, take place at around 15 GPa (GGA) and 28 GPa (GGA+U=5 eV), underestimating the corresponding experimental value of 50 GPa.

The total and partial DOS calculations show the electronic structures of the HS and LS phases. In the GGA+U calculations, with increasing pressure, the top of valence bands changes from strongly hybridized Fe 3d and O 2p orbitals to almost pure Fe 3d character. Whereas in the GGA method, the occupied states close to the Fermi energy are almost Fe 3d-electrons dominated. The analysis of the DOS and electronic charge-density calculations reveals that the delocalization of 3d electrons with increasing pressure leads to the HS→LS transition, accompanying a formation of a new d bond between two neighbor Fe atoms.

ACKNOWLEDGMENTS

This work was supported by Carl Trygress (CTS) and VR. We are also grateful to UPPMAX and NSC for the provision of computer supports.

*wei.luo@fysik.uu.se

[1] J. Badro, G. Fiquet, F. Guyot, J. P. Rueff, V. V. Struzhkin, G. Vankó, and G. Monaco, Science **300**, 789 (2003).
[2] J. F. Lin, V. V. Struzhkin, S. D. Jacobsen, M. Y. Hu, P. Chow, J. Kung, H. Liu, H. K. Mao, and R. J. Hemley, Nature (London) **436**, 377 (2005).
[3] S. Speziale, A. Milner, V. E. Lee, S. M. Clark, M. P. Pasternak, and R. Jeanloz, Proc. Natl. Acad. Sci. U.S.A. **102**, 17918 (2005).
[4] A. F. Goncharov, V. V. Struzhkin, and S. D. Jacobsen, Science **312**, 1205 (2006).
[5] J. Badro, J. P. Rueff, G. Vankó, G. Monaco, G. Fiquet, and F. Guyot, Science **305**, 383 (2004).
[6] J. F. Lin, G. Vankó, S. D. Jacobsen, V. Iota, V. V. Struzhkin, V. B. Prakapenka, A. Kuznetsov, and C. S. Yoo, Science **317**, 1740 (2007).
[7] J. C. Crowhurst, J. M. Brown, A. F. Concharov, and S. D. Jacobsen, Science **319**, 451 (2008).
[8] Y. Ding, D. Haskel, S. G. Ovchinnikov, Y. C. Tseng, Y. S. Orlov, J. C. Lang, and H. K. Mao, Phys. Rev. Lett. **100**, 045508 (2008).
[9] J. P. Rueff, C. C. Kao, V. V. Struzhkin, J. Badro, J. Shu, R. J. Hemley, and H. K. Mao, Phys. Rev. Lett. **82**, 3284 (1999).
[10] J. P. Rueff, M. Krisch, Y. Q. Cai, A. Kaprolat, M. Hanfland, M. Lorenzen, C. Masciovecchio, R. Verbeni, and F. Sette, Phys. Rev. B **60**, 14510 (1999).
[11] J. Badro, V. V. Struzhkin, J. Shu, R. J. Hemley, H. K. Mao, C. C. Kao, J. P. Rueff, and G. Shen, Phys. Rev. Lett. **83**, 4101 (1999).
[12] J. Badro, G. Fiquet, V. V. Struzhkin, M. Somayazulu, H. K. Mao, G. Shen, and T. Le Bihan, Phys. Rev. Lett. **89**, 205504 (2002).
[13] A. Shukla, J. P. Rueff, J. Badro, G. Vankó, A. Mattila, F. M. F. de Groot, and F. Sette, Phys. Rev. B **67**, 081101(R) (2003).
[14] C. S. Yoo *et al.*, Phys. Rev. Lett. **94**, 115502 (2005).
[15] J. P. Rueff, A. Mattila, J. Badro, G. Vankó, and A. Shukla, J.

Phys.: Condens. Matter **17**, S717 (2005).
[16] G. Vankó, J. P. Rueff, A. Mattila, Z. Németh, and A. Shukla, Phys. Rev. B **73**, 024424 (2006).
[17] S. Ohnishi, Phys. Earth Planet. Inter. **17**, 130 (1978).
[18] A. Kotani and S. Shin, Rev. Mod. Phys. **73**, 203 (2001).
[19] F. M. F. de Groot, Chem. Rev. (Washington, D.C.) **101**, 1779 (2001).
[20] F. M. F. de Groot, J. Electron Spectrosc. Relat. Phenom. **67**, 529 (1994).
[21] R. E. Cohen, I. I. Mazin, and D. G. Isaak, Science **275**, 654 (1997).
[22] Z. Fang, I. V. Solovyev, H. Sawada, and K. Terakura, Phys. Rev. B **59**, 762 (1999).
[23] S. A. Gramsch, R. E. Cohen, and S. Y. Savrasov, Am. Mineral. **88**, 257 (2003).
[24] T. Tsuchiya, R. M. Wentzcovitch, C. R. S. da Silva, and S. de Gironcoli, Phys. Rev. Lett. **96**, 198501 (2006).
[25] X. Jiang and G. Y. Guo, Phys. Rev. B **69**, 155108 (2004).
[26] M. Cococcioni, A. DalCorso, and S. de Gironcoli, Phys. Rev. B **67**, 094106 (2003).
[27] G. Rollmann, A. Rohrbach, P. Entel, and J. Hafner, Phys. Rev. B **69**, 165107 (2004).
[28] W. G. Wyckoff, *Crystal Structure* (Interscience, New York, 1948).
[29] E. R. Cowley, Can. J. Phys. **47**, 381 (1969).
[30] K. R. Rao, S. F. Trevino, and K. W. Logan, J. Chem. Phys. **53**, 4645 (1970).
[31] J. Santillán and Q. Williams, Phys. Earth Planet. Inter. **143-144**, 291 (2004).
[32] A. Mattila, J. Phys.: Condens. Matter **19**, 386206 (2007).
[33] L. S. Dubrovinsky, S. K. Saxena, P. Lazor, R. Ahuja, O. Eriksson, J. M. Wills, and B. Johansson, Nature (London) **388**, 362 (1997).
[34] P. E. Blöchl, Phys. Rev. B **50**, 17953 (1994).
[35] G. Kresse and J. Furthmüller, Phys. Rev. B **54**, 11169 (1996).
[36] G. Kresse and D. Joubert, Phys. Rev. B **59**, 1758 (1999).
[37] J. P. Perdew, J. A. Chevary, S. H. Vosko, K. A. Jackson, M. R. Pederson, D. J. Singh, and C. Fiolhais, Phys. Rev. B **46**, 6671 (1992).
[38] J. P. Perdew, J. A. Chevary, S. H. Vosko, K. A. Jackson, M. R. Pederson, D. J. Singh, and C. Fiolhais, Phys. Rev. B **48**, 4978 (1993).
[39] V. I. Anisimov, J. Zaanen, and O. K. Andersen, Phys. Rev. B **44**, 943 (1991).
[40] A. I. Liechtenstein, V. I. Anisimov, and J. Zaanen, Phys. Rev. B **52**, R5467 (1995).
[41] S. L. Dudarev, G. A. Botton, S. Y. Savrasov, C. J. Humphreys, and A. P. Sutton, Phys. Rev. B **57**, 1505 (1998).
[42] I. V. Solovyev, P. H. Dederichs, and V. I. Anisimov, Phys. Rev. B **50**, 16861 (1994).
[43] R. Grau-Crespo, I. de P. R. Moreira, F. Illas, N. H. de Leeuw, and C. R. A. Catlow, J. Mater. Chem. **16**, 1943 (2006).
[44] G. Schmitt, T. Gudde, and E. Strobel, Condensed from Paper No. 9 presented at CORROSION/96, 1996.